Boletim da Sociedade Astronômica Brasileira, **37**, no. 1, 234-237

Power spectrum large-angle analysis of the S-PLUS Quasar catalog

Maria Lopes & Felipe Avila

[1] Observatório Nacional, Rio de Janeiro. e-mail: marialopes@on.br, felipeavila@on.br

Abstract. Baryon acoustic oscillations (BAO) act as a cosmic ruler, allowing distance measurements throughout cosmic history to constrain cosmological parameters. In this work, we analyze the angular power spectrum of the S-PLUS DR4 quasar distribution at $\bar{z} = 2.201$, and find the shift parameter $\alpha = 1.0141^{+2.290}_{-3.273}$, given by the ratio of the angular diameter distance $D_A(z)$ to the sound horizon scale at the baryon drag epoch $r_d(z)$.

Resumo. As oscilações acústicas de bárions (BAO) atuam como uma régua cósmica, permitindo medições de distância ao longo da história cósmica para restringir parâmetros cosmológicos. Neste trabalho, analisamos o espectro de potência angular da distribuição de quasares do S-PLUS DR4 em $\bar{z} = 2,201$ e obtivemos o parâmetro de deslocamento $\alpha = 1,0141^{+2,290}_{-3,273}$, dado pela razão entre a distância angular $D_A(z)$ e a escala do horizonte acústico na época do último arrasto dos bárions.

Keywords. Cosmology: observations – large-scale structure of Universe – distance scale

1. Introduction

The large-scale structure of the Universe preserves cosmological information from the era of strong coupling of the hot plasma of photons and baryons in the primordial Universe. The interaction between the photon-baryon coupled fluid and the dark matter overdensities produced the baryon acoustic oscillations (BAO), spherical sound waves that propagated through the photon-baryon plasma until the end of the drag epoch, slightly after recombination, when the Universe had cooled enough for photons to decouple from baryons, allowing protons to capture free electrons and form neutral hydrogen atoms (Peebles & Yu 1970; Sunyaev & Zeldovich 1970). After this process, baryons effectively decoupled from radiation and the acoustic waves freeze out, forming spherical shells of matter overdensity at a given distance from the center, then starting to act as seeds for galaxies and clusters (Seo & Eisenstein 2007). Thus, this mechanism imprints a well-defined characteristic scale in the matter distribution, known as the sound horizon, r_d, with approximately 150 Mpc (Planck Collaboration et al. 2020), which corresponds to the maximum comoving distance traveled by the acoustic waves until the end of the baryon drag epoch (Dodelson 2003).

As a cosmic standard ruler, BAO measurements allow us to determine distances and constrain cosmological parameters. In the analysis of the distribution of matter projected onto the sky (2D), the BAO signature appears as a ring of angular radius $\theta_{\rm BAO}(z)$, which relates to the 3D physical scale. The transverse BAO scale has already been measured in the literature using different cosmic tracers, such as blue galaxies, bright red galaxies, emission line galaxies, and quasars (Avila et al. 2025c; Ribeiro et al. 2025; Ferreira et al. 2025; de Carvalho et al. 2021; Carvalho et al. 2020). In astronomical surveys, the projected distribution of these tracers is analyzed in redshift bins using the angular correlation function (2PACF) or the angular power spectrum (APS).

Quasars act as effective tracers of large-scale structures in the distant universe due to their high luminosity (Nakazono et al. 2023; de Carvalho et al. 2018, 2020). Various astronomical surveys have been dedicated to observing quasars, such as the spectroscopic surveys Sloan Digital Sky Survey (SDSS)(York et al. 2000), extended Baryon Oscillation Spectroscopic Survey (eBOSS)(Dawson et al. 2016), and Dark Energy Spectroscopic Instrument (DESI)(DESI Collaboration et al. 2016), which provide accurate redshifts, and photometric surveys such as the Dark Energy Survey (DES)(Dark Energy Survey Collaboration et al. 2016), Legacy Survey of Space and Time (LSST0)(LSST Science Collaboration et al. 2009), and Southern Photometric Local Universe Survey (S-PLUS)(Mendes de Oliveira et al. 2019), which detect millions of quasar candidates via multiband imaging and provide estimated redshifts using machine learning. The main advantage of using photometric data is that it supports large-volume surveys, which are essential for mapping the distribution of matter on cosmological scales. In this work, our goal is to analyze the angular power spectrum of the projected distribution of quasars to detect and characterize the transverse BAO scale. For this, we will use photometric data from the S-PLUS DR4 quasar catalog, which will allow us to infer the transverse BAO scale from the angular clustering signal of quasars.

2. Observational data

We used the S-PLUS Quasar Catalog (QuCatS) provided by Nakazono et al. (2023), which contains 645,980 quasar candidates with a classification probability greater than 80%. This sample reaches a photometric depth of r < 21.3 in the r band and has good photometric quality in the detection images. The catalog covers approximately 3,000 square degrees and includes information such as equatorial coordinates, photometric redshifts with uncertainties, classification probabilities, and other relevant data. For the analysis of the angular power spectrum, it is necessary to select a connected area with good angular extension and good numerical density. Thus, we selected the region in violet in Figure 1, which meets the aforementioned requirements. Additionally, to obtain a BAO signal in the distribution of tracers, we need to define a spherical shell with a narrow Δz thickness, as this ensures that all galaxies are approximately at the same comoving distance, projecting the fixed physical scale of the BAO at a well-defined angle and not diluting the signal. In the case of quasars, due to the low overall numerical density of the catalog compared to other surveys, the size of the shell must be compromised, as there is insufficient density in very thin shell. Therefore, to compose our final analysis sample, we selected the quasars located within the area in violet, and applied a cut in

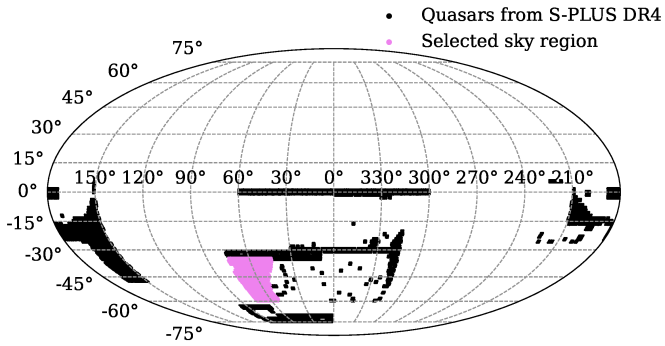

Figure 1. Sky coverage of the S-PLUS Quasar Catalog (gray) and the selected sample (violet)) in equatorial coordinates.

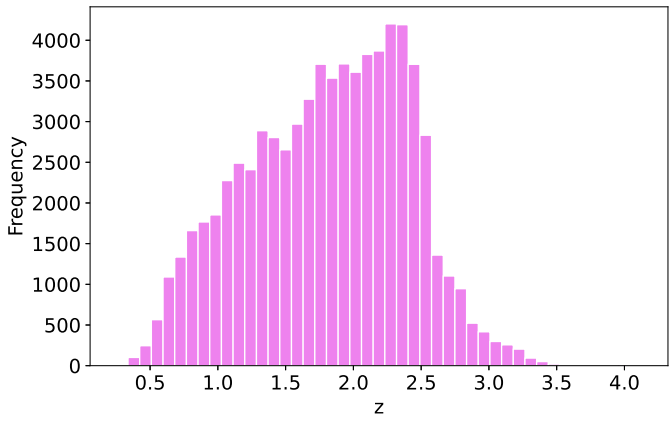

Figure 2. Redshift distribution of the selected region.

the photometric redshift (`z_mean`) of the catalog according to the redshift distribution in Figure 2, restricting the sample to the interval $1.951 \leq z \leq 2.451$ ($\Delta z = 0.5$).

3. Methodology

3.1. The angular power spectrum

To obtain the angular power spectrum, we constructed a density fluctuation map of quasar using celestial sphere discretization with HEALPix[1] (Górski et al. 2005). The celestial sphere was discretized with resolution $N_{side} = 128$, in a way that the quasar density contrast, $\delta_q(\theta, \phi)$, is computed for each direction i in the sky (pixel) using the equation

$$\delta_q^i(\theta, \phi) = \frac{{n_q}^i(\theta, \phi) - \langle n_q \rangle}{\langle n_q \rangle}, \tag{1}$$

where $n_q(\theta, \phi)$ is the number count of objects in that direction and $\langle n_q \rangle$ denotes the average number density of quasars over the observed sky. These values are used to construct the sky map of density fluctuation and this map can be decomposed into pseudo-spherical harmonics, allowing us to compute the angular power spectrum as previously described.

So, as the sample does not cover the entire sky, we used the publicly available code NaMaster[2] to correct the partial sky coverage to estimate the angular power spectrum relies on the assumption

$$\langle \hat{C}_\ell(\delta_q(\hat{n})) \rangle = \sum_{\ell'} M_{\ell\ell'} \, C_{\ell'}(\delta_q(\hat{n})), \tag{2}$$

where $\hat{C}_\ell$ denotes the observed (pseudo) angular power spectrum of the quasar overdensity field, $C_{\ell'}$ is the underlying true sky power spectrum, and $M_{\ell\ell'}$ is the mode mixing matrix, which corrects couplings between multipoles in the angular power spectrum caused by an inhomogeneous sky mask.

3.2. The Theoretical Covariance Matrix

To obtain uncertainties in the measured angular power spectra, an accurate estimate of the covariance matrix is essential. This is crucial in cosmological analyzes, as it directly defines the precision and statistical significance of the constraints on cosmological parameters (Avila et al. 2025c).

In our analysis, performed on a partial sky coverage, we adopted a Gaussian covariance matrix based on the approximation f_{sky} (Camacho et al. 2019), defined as

$$\mathrm{Cov}^{ij}_{\ell\ell'} \equiv \left\langle C^i_\ell C^j_{\ell'} \right\rangle - \left\langle C^i_\ell \right\rangle \left\langle C^j_{\ell'} \right\rangle = \frac{2}{f_{\rm sky}\,\Delta\ell\,(2\ell+1)} \left(C^{ij}_\ell + \frac{\delta_{ij}}{\bar{n}_i} \right)^2 \delta_{\ell\ell'}, \tag{3}$$

where C^{ij}_ℓ represents the theoretical power spectrum crossed between photo-z bins i and j, $\bar{n}_i$ is the average density of quasars in bin i (shot noise term), Δ_ℓ is the bin size in multipoles, f_{sky} is the effective fraction of the observed sky and $\delta_{\ell\ell'}$ and δ_{ij} are the Kronecker deltas that ensure diagonality in the Gaussian approximation for surveys with high statistics.

3.3. Angular Power Spectrum Fitting and BAO Measurement

Our goal is to determine the angular BAO scale, from our quasar sample, which is related to the angular diameter distance $D_A(z)$. To reduce sensitivity to nonlinear effects such as bias and redshift-space distortions, we adopt a template-fitting approach (Camacho et al. 2019). The angular power spectrum was modeled by projecting the theoretical template of P(k)

$$P_{\rm temp}(k, z) = [P_{\rm lin}(k, z) - P_{\rm nw}(k, z)]\, e^{-k^2\Sigma^2_{\rm nl}} + P_{\rm nw}(k, z), \tag{4}$$

where $P(k, z)_{lin}$ is the linear power spectrum, $P(k, z)_{nw}$ is the linear spectrum no-wiggles obtained from the Eisenstein-Hu parametrization (Eisenstein & Hu 1998), both obtained with the public code from Core Cosmology Library (CCL)[3], and the nonlinear damping scale $\Sigma_{nl} = 5.2$ Mpc/h which we set at the value used in the literature. This P^{temp} is designed using the Limber approximation (Limber 1953) to obtain the template C^{temp}. Therefore, our default template for angular power spectrum is given by

$$C(\ell) = B_0^2\, C^{temp}(\ell/\alpha) + A_0 + A_1\ell + \frac{A_2}{\ell^2}, \tag{5}$$

where α is the shift parameter, defined as

$$\alpha \equiv \frac{D_A(z)/r_d}{(D_A(z)/r_d)_{\rm fid}}, \tag{6}$$

which quantifying how the measurement deviates from the expectation in the fiducial cosmology. In this work, we adopt the

[1] `https://healpy.readthedocs.io/en/latest/`
[2] `https://github.com/LSSTDESC/NaMaster`
[3] `https://github.com/LSSTDESC/CCL`

Table 1. Values extracted from Planck Collaboration (Planck Collaboration et al. 2020)). Used in CCL for P(k,z) in the quasar bin $z \in [1.951, 2.451]$.

Parameter	Value
Baryon density (Ω_b)	0.0494
Dark matter density (Ω_c)	0.2656
Dimensionless Hubble constant (h)	0.6727
Amplitude of the matter fluctuation (σ_8)	0.8120
Primordial spectral index (n_s)	0.9649

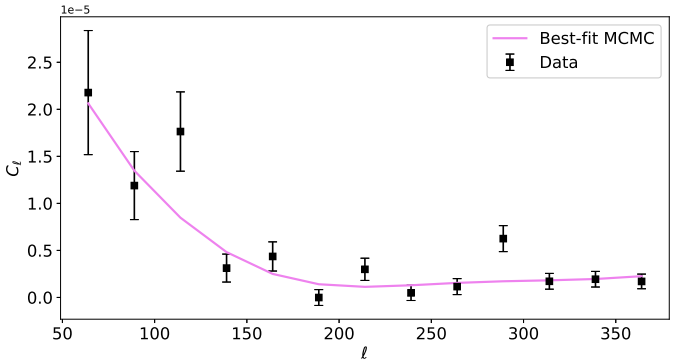

Figure 3. The black dots represent the data and the solid violet line corresponds to the best-fit model.

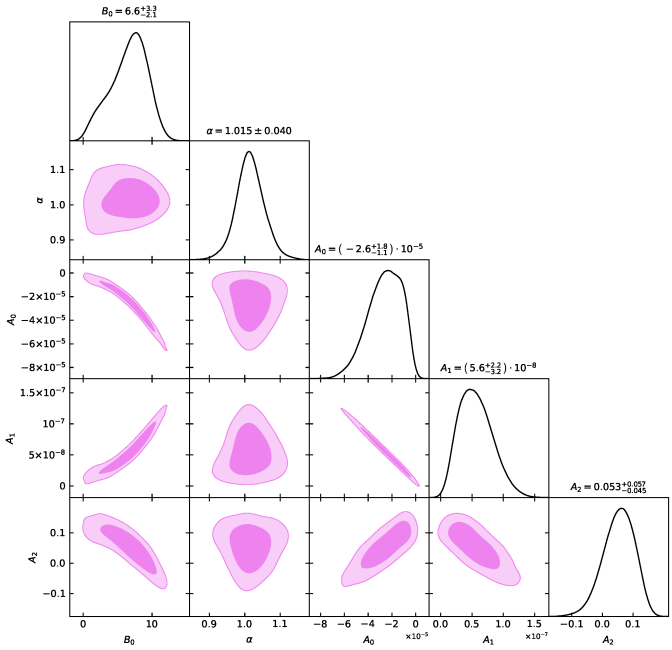

Figure 4. Triangle plot showing the posterior distributions of the cosmological parameters obtained in this work. The contours correspond to the 68% and 95% confidence levels.

ΛCDM model as our fiducial cosmology, using the following Planck parameters (Planck Collaboration et al. 2020) listed in Table 1.

We chose this template to fit the angular power spectrum because it allows us to isolate the BAO feature while accounting for the overall shape of the spectrum, including shot noise, scale-dependent bias, and other smooth contributions. In addition, we use the term B_0^2 differently from that already used in the literature, because it better fits our data.

We use Markov Chain Monte Carlo (MCMC) methods to fit the model parameters. For the MCMC we used uniform priors for the parameters $B_0 \in [0.1, 20]$, $A_0 \in [-5 \times 10^7, 5 \times 10^7]$, $A_1 \in [-8 \times 10^{10}, 8 \times 10^{10}]$, and $A_0 \in [-9 \times 10^{12}, 9 \times 10^{12}]$, combined with a Gaussian prior for $\alpha \sim \mathcal{N}(\mu = 1.0,\ \sigma = 0.05)$.

4. Preliminary results

In our analysis, we considered multipoles $\ell > 50$ and used a bin width of $\Delta\ell = 25$. The resulting angular power spectrum is shown in Figure 3 in black points, where the error bars are computed using the theoretical covariance matrix. In the same figure and Figure 4 we show the results from the MCMC chains, the best-fit model and the corner plot displaying the marginalized posterior distributions of the free parameters, respectively.

We find $\alpha = 1.0141^{+2.290}_{-3.273}$ with χ^2/dof=3.2, consistent with the expected ΛCDM theoretical value within the asymmetric uncertainties reported at the level of 1σ. This result suggests low agreement between the observed data and the theoretical model we used in our analysis. In a study currently in preparation (Lopes et al. 2026) using the same QuCatS catalog from S-PLUS, similar results were obtained with both the theoretical covariance matrix and log-normal simulations, ruling out underestimation of uncertainties as the main cause of inflation in reduced χ^2. Different tests with different multipole binning schemes confirmed that the current choice offers the best fit, avoiding excessive noise in the alternatives evaluated. We believe that the discrepancy stems from systematic contamination in the photometric nature of the data, possibly due to photometric redshift effects, for example. In the same study cited, several analyses are being conducted to investigate the impact of photo-z, such as sample splitting.

5. Conclusions and perspectives

Using quasars from the S-PLUS DR4 catalog $\bar{z} = 2.201$ we obtained a BAO signature in the angular power spectrum, with $\alpha = 1.0141^{+2.290}_{-3.273}$, consistent with the standard ΛCDM model within uncertainties. However, the reduced $\chi^2 = 3.2$ indicates systematic discrepancies likely related to the photometric nature of the data.

These preliminary results are part of ongoing analyses by Lopes et al. (2026). New MCMC fits testing alternative templates, log-normal mock catalogs, robustness tests, statistical significance quantification, consistency checks, and the impact of photometric redshift sampling are currently underway.

Acknowledgements. ML acknowledges to CAPES, and FA thanks to Fundação Carlos Chagas Filho de Amparo à Pesquisa do Estado do Rio de Janeiro (FAPERJ), Processo SEI-260003/001221/2025, for the financial support under which this work was carried out.

References

Alves, D. et al. 2026, in preparation
Avila, F. et al. 2018, JCAP, 12, 041
Avila, F. et al. 2022, MNRAS, 509, 2994
Avila, F. et al. 2023, Braz. J. Phys., 53, 49
Avila, F. et al. 2025a, Phys. Lett. B, 867, 139606
Avila, F. et al. 2025b, Universe, 11, 307
Avila, F. et al. 2025c, arXiv:2510.15650
Camacho, H. et al. 2019, MNRAS, 487, 3870
Carvalho, G. C. et al. 2020, Astropart. Phys., 119, 102432
Dark Energy Survey Collaboration et al. 2016, MNRAS, 460, 1270
Dawson, K. S. et al. 2016, AJ, 151, 44
de Carvalho, E. et al. 2018, JCAP, 04, 064
de Carvalho, E. et al. 2020, MNRAS, 492, 4469
de Carvalho, E. et al. 2021, A&A, 649, A20
DESI Collaboration et al. 2016, arXiv:1611.00036

Dias, B. L. et al. 2023, MNRAS, 526, 3219
Dodelson, S. 2003, Modern Cosmology, Elsevier
Eisenstein, D. J. & Hu, W. 1998, ApJ, 496, 605
Ferreira, P. S. et al. 2025, arXiv:2510.02144
Franco, C. et al. 2024, MNRAS, 527, 7400
Franco, C. et al. 2025a, MNRAS, 537, 897
Franco, C. et al. 2025b, ApJ, 993, 133
Górski, K. M. et al. 2005, ApJ, 622, 759
Lazarin, M. et al. 2026, in preparation
Limber, D. N. 1953, ApJ, 117, 134
Lopes, M. et al. 2024, ApJ, 967, 47
Lopes, M. et al. 2025, A&A, 694, A77
Lopes, M. et al. 2026, in preparation
LSST Science Collaboration et al. 2009, arXiv:0912.0201
Marques, G. et al. 2020, JCAP, 05, 052
Mendes de Oliveira, C. et al. 2019, MNRAS, 489, 241
Mokeddem, R. et al. 2026, PDU, 51, 102185
Nakazono, L. et al. 2023, MNRAS, 531, 327
Novaes, C. P. et al. 2016, MNRAS, 461, 1363
Nunes, R. C. et al. 2020, EPJC, 80, 1025
Oliveira, F. et al. 2024, EPJC, 84, 636
Oliveira, F. et al. 2025a, PDU, 49, 101996
Oliveira, F. et al. 2025b, JCAP, 12, 007
Peebles, P. J. E. & Yu, J. T. 1970, ApJ, 162, 815
Planck Collaboration et al. 2020, A&A, 641, A6
Ribeiro, U. et al. 2025, arXiv:2506.08288
Seo, H.-J. & Eisenstein, D. J. 2007, ApJ, 665, 14
Sunyaev, R. A. & Zeldovich, Ya. B. 1970, Ap&SS, 7, 3
York, D. G. et al. 2000, AJ, 120, 1579